Spectroscopy of samarium isotopes in the *sdg* interacting boson model

Y. D. Devi and V. K. B. Kota
Physical Research Laboratory, Ahmedabad 380 009, India
(Received 1 April 1991)

Successful spectroscopic calculations for the 0_1^+, 2_1^+, and 4_1^+ levels in $^{146-158}$Sm are carried out in *sdg* boson space with the restriction that the *s*-boson number $n_s \geq 2$ and the *g*-boson number $n_g \leq 2$. Observed energies, quadrupole and magnetic moments, $E2$ and $E4$ transition strengths, nuclear radii, and two-nucleon transfer intensities are reproduced with a simple two-parameter Hamiltonian. For a good simultaneous description of ground, β, and γ bands, a Hamiltonian interpolating the dynamical symmetries in the *sdg* model is employed. Using the resulting wave functions, in ^{152,154}Sm, the observed $B(E4;0_1^+ \rightarrow 4_\gamma^+)$ values are well reproduced and $E4$ strength distributions are predicted. Moreover, a particular ratio $\mathcal{R}$ involving two-nucleon transfer strengths showing a peak at neutron number 90 is well described by the calculations.

PACS number(s): 21.60.Ev, 21.60.Fw, 27.70.+q, 21.10.Re

I. INTRODUCTION

In the past few years considerable experimental data on $E4$ matrix elements [1–3] and strength distributions [4–6] has accumulated and their theoretical understanding (using models or microscopic theories) is a challenging problem. One of the models well suited for this purpose is the *sdg* interacting boson model (*sdg*IBM or simply *g*IBM); here the IBM with $s(l=0)$ and $d(l=2)$ bosons is extended to include $g(l=4)$ bosons. An up-to-date survey of the *g*IBM and its success has been documented recently [7]. Some of the growth points in this model are (i) selection rules [8,9] in $E2$ data involving $K^\pi=4^+$ and 3^+ bands in ^{156}Gd and ^{178}Hf, $E1$ data in ^{218}Ra; (ii) identification of dynamical symmetries [10] and the study of the corresponding geometric shapes [11], occurrence of low-lying $K^\pi=1^+$, 3^+ bands and two types (two phonon, hexadecupole) of $K^\pi=4^+$ rotational bands [12]; (iii) good description of the variety of rotational bands [13] in ^{168}Er, two-particle transfer data [14] in ^{166}Er$(t,p)^{168}$Er; (iv) the $1/N$ expansion technique and its application [15] in explaining *g*-factor variation with respect to L in ^{166}Er; (v) quantitative description [4] of $E4$ strength distributions in ^{156}Gd and ^{150}Nd; (vi) simple description [16] of spherical-deformed phase transition in Sm isotopes as a boson number effect; and (vii) preliminary work [7,17] on interactions in *sdg* space. In spite of all these new results, the progress in applying *g*IBM in a wide variety of situations is slow because (i) the general *g*IBM Hamiltonian contains too many parameters, three single-particle energies (SPE), and 32 two-body matrix elements (TBME), (ii) the matrix dimensions in *sdg* space are very large (see Table I in Sec. II), and (iii) except for the SU(3) and U(6)⊕U(9) limits, the applicability of the other *g*IBM dynamical symmetries [10] [SU(5), SU(6), O(15), U(1)⊕U(14), U(5)⊕U(10)] is not clear. Most of the calculations to date are confined to variational methods, truncations based on *sdg* SU(3) or coupling a single *g* boson to *sd*IBM core nucleus. However, with the development of the package SDGIBM1 [7] which allows one to construct and diagonalize *g*IBM matrices in spherical $(n_s n_d n_g)$ basis and produce occupancies, two-nucleon transfer strengths, and $E2$, $M1$, and $E4$ matrix elements, it is feasible to explore and apply this model in detail. This coupled with the fact that a simple Hamiltonian based on *g*IBM symmetries (with 6–8 free parameters) appears to reproduce the experimental data makes the *sdg* model a powerful tool for analyzing $E4$ properties in nuclei. It is our purpose here to demonstrate the same and to this end we choose Sm isotopes as they are sufficiently complex.

Recently Otsuka and Sugita (OS) analyzed [16] the energies and $E2$ properties of 0_1^+, 2_1^+, and 4_1^+ levels of Sm isotopes in *sdg* framework employing variational (with projection) method. They demonstrated that the observed spherical-deformed shape phase transition (with respect to neutron number) in these isotopes is due to boson number N. In the *sd*IBM calculations of Scholten *et al.* [18] boson-number-dependent *d*-boson energy had to be used. However, it is seen that the variational calculations do not reproduce [19] the β- and γ-band energies and other related properties with the same simple Hamiltonian that reproduced the phase transition (see Sec. III). Thus a good description of the excited bands calls for detailed *g*IBM calculations and with this one can predict reliably the $E4$ properties of Sm isotopes. It should be pointed out that *sd*IBM calculations necessarily fail in describing $E4$ properties (see, for example, Refs. [1,4]). Keeping these in mind, first we repeated OS calculations in the spherical basis to establish that the variational results are essentially kept intact in the matrix diagonalization approach and also extend the calculations to other observables such as $B(E4\uparrow)$'s, *g* factors, nuclear radii, and two-nucleon transfer strengths. The results are described in Sec II. Having shown that a truncated spherical basis is meaningful we employ a Hamiltonian based on *g*IBM dynamical symmetries (with six free parameters) to reproduce β- and γ-band energies and related properties. In Sec. III detailed calculations for ^{148}Sm, ^{150}Sm, ^{152}Sm, and ^{154}Sm are reported. For ^{152,154}Sm iso-

topes $B(E4)$ data ($0_1^+ \rightarrow 4_1^+, 0_1^+ \rightarrow 4_\gamma^+$) exists [3] and the effective charge that is used to reproduce the $B(E4;0_1^+ \rightarrow 4_1^+)$ predicts the $B(E4;0_1^+ \rightarrow 4_\gamma^+)$ values close to the data. With this agreement, reliable predictions for $E4$ distributions in ^{152,154}Sm are made. Moreover, a particular ratio $\mathcal{R}$ (see Sec. III) involving two-nucleon transfer (TNT) strengths which shows a peak at neutron number 90 is well described by the calculations. These results and the predictions for the properties of 1_1^+ levels in ^{152,154}Sm are also given in Sec. III. Finally, Sec. IV gives some concluding remarks.

II. SPECTROSCOPY OF LOW-LYING LEVELS IN Sm ISOTOPES: SIMPLE *g*IBM CALCULATIONS

The 0_1^+, 2_1^+, and 4_1^+ levels of doubly even Sm isotopes $^{146-158}$Sm are studied employing a simple two-parameter Hamiltonian

$$H = F\{\varepsilon_d n_d + \varepsilon_g n_g + \kappa Q^2 \cdot Q^2\} , \tag{1}$$

where

$$Q^2 = (d^\dagger \tilde{s} + s^\dagger \tilde{d})^2 - \frac{11\sqrt{10}}{28}(d^\dagger \tilde{d})^2 + \frac{9}{7}(d^\dagger \tilde{g} + g^\dagger \tilde{d})^2 + \frac{3\sqrt{55}}{14}(g^\dagger \tilde{g})^2 . \tag{2}$$

In (1), F is the parameter which scales the spectrum, κ is the strength of the quadrupole-quadrupole force, and ε_d and ε_g are d- and g-boson energies, respectively. In the calculations reported later ε_d and ε_g are taken to be the same for all Sm isotopes and hence F and κ are the only two free parameters in (1). In (1) and (2) Q^2 is the *g*IBM SU(3) quadrupole operator. The Hamiltonian (1) is diagonalized (using the package SDGIBM1) in a truncated set of spherical basis states $|n_s; n_d v_d \alpha_d L_d; n_g v_g \alpha_g L_g; L_f\rangle$, where n_d and n_g are boson numbers, v_d and v_g seniority quantum numbers, and L_d and L_g are angular momentum quantum numbers for d and g bosons, respectively. The labels α_d and α_g are used to specify the states completely and the final angular momentum $\mathbf{L}_f = \mathbf{L}_d + \mathbf{L}_g$. With n_s being the s-boson number, $N = n_s + n_d + n_g$, where N is the total number of bosons. For $^{146-158}$Sm, N takes values 7–13 ($N_\pi = 6$ and $N_\nu = 1-7$ where π and ν stand for proton and neutron bosons). In all the calculations the basis states are restricted such that $n_s \geq 2$ and $n_g \leq 2$. This truncation scheme is adopted based on the following facts: (i) in *sd*IBM vibrational [SU(5)] limit the ground state (g.s.) s-boson occupancy $\langle \hat{n}_s \rangle^{\text{g.s.}} = N$ and in the rotational [SU(3)] limit $\langle \hat{n}_s \rangle^{\text{g.s.}} = N/3 \simeq 3-4$, and (ii) the microscopic theory (based on Hartree-Fock-Bogoliubov intrinsic states) of Pannert *et al.* [20] shows that even for a well-deformed nucleus ^{154}Sm n_g takes a maximum value of 2 ($n_g \leq 2$). Moreover, calculations relaxing the above restrictions (allowing for $n_s \geq 0$ or 1, $n_g \leq 3$ or 4) showed negligible improvements in energies and $B(E2)$ values. Table I gives the matrix dimensions for $L \leq 6$. The results of the calculations for energies, $E2$, $M1$, and $E4$ properties, isomer and isotope shifts, and TNT are described in Secs. II A–II F and a summary with comments is given in Sec. II G.

A. Energies

The parameters in the Hamiltonian (1) are chosen to be $\varepsilon_d = 1.3$ MeV, $\varepsilon_g = 1.8$ MeV, $F = 1.0$, and $\kappa = -0.0375$ MeV for $^{146-158}$Sm, and the values of (F,κ) are changed to $F = 0.7$ and $\kappa = -0.04875$ MeV for $^{152-158}$Sm. With these two sets of parameters, properties of $^{146-158}$Sm are calculated. The set used for $^{146-150}$Sm was employed before by OS in their variational calculations (see also Sec. II G). Excitation energies (E_x) of 2_1^+ and 4_1^+ levels are shown in Fig. 1(a) and the ratio $R = E_x(4_1^+)/E_x(2_1^+)$ is shown in Fig. 1(b). The vibration-rotation phase transition is clearly seen in theory and experiment in both the energies and the ratio R; the ratio R changes from vibrational $R = 2$ to rotational $R = 10/3$ values as we move from $^{146-148}$Sm to $^{154-158}$Sm. In *g*IBM one can also calculate binding energies. For a fixed proton-boson number N_π, the two-nucleon separation energies are given by [16,18]

$$S_{2n} = A_0 + A_1 N_\nu + E_{\text{g.s.}}(N_\pi, N_\nu) - E_{\text{g.s.}}(N_\pi, N_\nu + 1) , \tag{3}$$

where $E_{\text{g.s.}}$ is the ground-state energy calculated with the Hamiltonian (1) and A's are free parameters. The calculated separation energies are shown in Fig. 1(c). The values of the parameters obtained from a fit to data are $A_0 = 15.23$ MeV and $A_1 = -0.614$ MeV. The sudden discontinuity from the straight-line behavior in the phase-transition domain is well reproduced by the calculations and the parameters A's are consistent with those of Refs. [16,18].

B. $E2$ transitions and quadrupole moments

Following OS, the $E2$ transition operator is chosen to be

TABLE I. Dimensionalities in *sdg* space with the restriction $n_s \geq 2$ and $n_g \leq 2$.

Nucleus	N/L	0^+	1^+	2^+	3^+	4^+	5^+	6^+
^{146}Sm	7	18	14	43	34	53	38	46
^{148}Sm	8	29	26	73	63	95	73	88
^{150}Sm	9	41	44	114	105	153	127	149
^{152}Sm	10	58	67	167	160	231	200	235
^{154}Sm	11	77	97	231	231	328	295	347
^{156}Sm	12	100	132	309	315	447	413	487
^{158}Sm	13	125	174	398	416	586	555	656

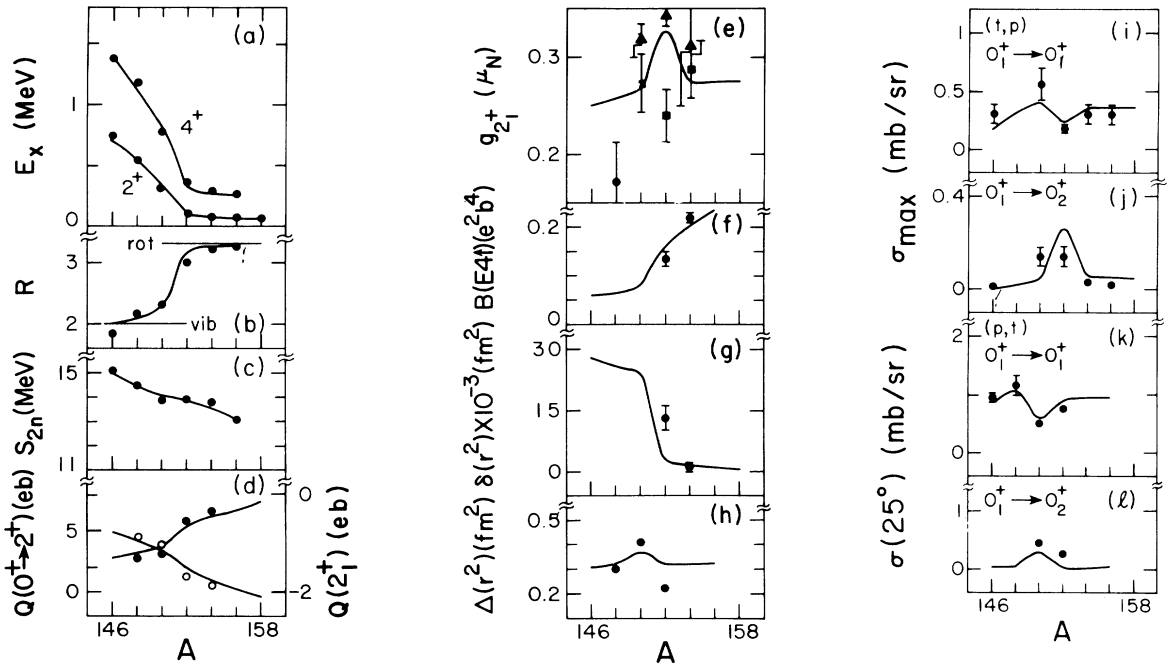

FIG. 1. Comparison of properties of 0_1^+, 2_1^+, and 4_1^+ states, between calculated (full line) and experimental (points): (a) excitation energies (E_x) of 2_1^+ and 4_1^+ states [21]; (b) ratio $R=E_x(4_1^+)/E_x(2_1^+)$; (c) two-neutron separation energies [22] S_{2n}; (d) transition moments of $0_1^+ \to 2_1^+$ (closed circles) [23]; and static moments of 2_1^+ states (open circles) [23,24]; (e) g factors [25]; (f) $B(E4\uparrow)=B(E4;0_1^+ \to 4_1^+)$ values [26]; (g) isomer shifts [27]; (h) isotope shifts [28]; (i) $0_1^+ \to 0_1^+$ (t,p) transfer cross sections [31]; (j) $0_1^+ \to 0_2^+$ (t,p) transfer cross sections [31]; (k) $0_1^+ \to 0_1^+$ (p,t) transfer cross sections [32]; (l) $0_1^+ \to 0_2^+$ (p,t) transfer cross sections [32].

$$T^{E2}=e_2 Q^2 , \tag{4}$$

where Q^2 is the gIBM SU(3) quadrupole operator defined in Eq. (2) and e_2 is the effective charge. Figure 1(d) shows the transition moments $Q(0_1^+ \to 2_1^+)=[(16\pi/5)B(E2;0_1^+ \to 2_1^+)]^{1/2}$ and the static moments $Q(2_1^+)$. The value of the effective charge obtained from the fit to $Q(2_1^+)$ is $e_2=0.113$ e b. The phase transition here manifests itself in a sharp increase in the value of the transition moment $Q(0_1^+ \to 2_1^+)$ which is reproduced by the calculation.

C. Magnetic g factors

In gIBM, the general one-body $M1$ operator is

$$T^{M1}=\sqrt{3/4\pi}\sqrt{10}[\alpha(d^\dagger \tilde{d})^1+\sqrt{6}\beta(g^\dagger \tilde{g})^1] . \tag{5}$$

In terms of the parameters α and β, the effective g factor for the 2_1^+ level ($g_{2_1^+}^{\rm eff}$) is

$$g_{2_1^+}^{\rm eff}=\alpha+\sqrt{60}\{\beta-\alpha\}*\frac{G}{2} ,$$
$$G=\begin{bmatrix}2 & 2 & 1\\ 2 & -2 & 0\end{bmatrix}\langle 2_1^+\|(g^\dagger \tilde{g})^1\|2_1^+\rangle . \tag{6}$$

In (6) $\begin{bmatrix}\cdots\end{bmatrix}$ stands for the Wigner's 3-j symbol. The parameters α and β are determined by fitting the g-factor data for the 2_1^+ states and the values obtained are $\alpha=0.21\mu_N$ and $\beta=0.45\mu_N$. These values of (α,β) are quite different from $(0.55\mu_N, 0.13\mu_N)$ and $(\sim 1\mu_N, \sim 1\mu_N)$ determined for ^{168}Er [13] and ^{156}Gd [4]. It is worth mentioning that due to large scatter in the g-factor data for Sm isoptoes [see Fig. 1(e)] the (α,β) values given above are not unique ($\alpha \simeq \beta \simeq 0.28\mu_N$ also gives a good fit) and the real test for them comes from $B(M1;1_1^+ \to 0_1^+)$ data which is not yet available (note that 1_1^+ is a gIBM symmetric 1^+ level but not a scissors 1^+ level). The results for g factors calculated with the above set ($\alpha=0.21\mu_N$, $\beta=0.45\mu_N$) are shown in Fig. 1(e). Here the data show large deviations from the linear behavior of the "standard" value of Z/A and the calculations reproduce the observed trend. In the sdIBM calculations a two-body $M1$ operator has to be employed [18] to obtain agreement with data.

D. $E4$ transitions

The general $E4$ operator in gIBM can be written as

$$T^{E4}=e_4\{(s^\dagger \tilde{g}+g^\dagger \tilde{s})^4+\eta_1(d^\dagger \tilde{d})^4 +\eta_2(d^\dagger \tilde{g}+g^\dagger \tilde{d})^4+\eta_3(g^\dagger \tilde{g})^4\} . \tag{7}$$

In the present calculations the η's in (7) are taken to be equal to the matrix elements of the $r^4Y^{(4)}$ operator in the sdg harmonic oscillator basis [4] and the only free parameter is e_4. Thus $\eta_1=19\sqrt{5}/28$, $\eta_2=-5\sqrt{11}/14$, and $\eta_3=3\sqrt{143}/28$. The $B(E4\uparrow)$ for $0_1^+ \to 4_1^+$ determine the value of the effective charge e_4 to be $e_4=0.034$ e b^2; the results for $B(E4\uparrow)$ are shown in Fig. 1(f). It can be seen that there is a marked rise in the $B(E4\uparrow)$ values in the phase-transition domain from vanishing values at the vi-

brational end to fairly large values for the rotational nuclei. The operator in (7) with the above value for e_4 effective charge predicts $B(E4;0_1^+\rightarrow 4_\gamma^+)$ in close agreement with data [3]; see Sec. III.

E. Nuclear radii: Isomer and isotope shifts

In the *sdg* space the most general one-body rank-zero operator can be written as

$$T^{(0)}=a_0+a_1\hat{N}+a_2\hat{n}_d+a_3\hat{n}_g \ . \tag{8}$$

The structure of $T^{(0)}$ can be used to calculate nuclear radii [18],

$$\langle \hat{r}^2\rangle^{(N)}_{L_I^+}=\langle r_0^2\rangle_{(c)}+\gamma_1\hat{N}+\gamma_2\langle \hat{n}_d\rangle^{(N)}_{L_I^+}+\gamma_3\langle \hat{n}_g\rangle^{(N)}_{L_I^+} \ , \tag{9}$$

where $\langle \hat{r}^2\rangle^{(N)}_{L_I^+}$ represents the mean square radius of a nucleus with N bosons in the state L_I^+, $\langle r_0^2\rangle_{(c)}$ is a constant term which represents the contribution due to the closed shells, and $\langle \hat{n}_d\rangle$ and $\langle \hat{n}_g\rangle$ are the expectation values of the d- and g-boson number operators $\hat{n}_d$ and $\hat{n}_g$, respectively. The isomer shift $\delta(r^2)$ is defined to be the difference in the mean square radii of 2_1^+ and the ground 0_1^+ states,

$$\begin{aligned}\delta(r^2)&=\langle \hat{r}^2\rangle^{(N)}_{2_1^+}-\langle \hat{r}^2\rangle^{(N)}_{0_1^+}\\ &=\gamma_2(\langle \hat{n}_d\rangle^{(N)}_{2_1^+}-\langle \hat{n}_d\rangle^{(N)}_{0_1^+})+\gamma_3(\langle \hat{n}_g\rangle^{(N)}_{2_1^+}-\langle \hat{n}_g\rangle^{(N)}_{0_1^+}) \ .\end{aligned} \tag{10}$$

Similarly, the isotope shift $\Delta(r^2)$ is defined as the difference in the mean square radii of the ground states of the two neighboring even-even nuclei,

$$\begin{aligned}\Delta(r^2)&=\langle \hat{r}^2\rangle^{(N+1)}_{0_1^+}-\langle \hat{r}^2\rangle^{(N)}_{0_1^+}\\ &=\gamma_1+\gamma_2[\langle \hat{n}_d\rangle^{(N+1)}_{0_1^+}-\langle \hat{n}_d\rangle^{(N)}_{0_1^+}]\\ &\quad+\gamma_3[\langle \hat{n}_g\rangle^{(N+1)}_{0_1^+}-\langle \hat{n}_g\rangle^{(N)}_{0_1^+}] \ .\end{aligned} \tag{11}$$

The values of γ_1, γ_2, and γ_3 in Eqs. (10) and (11) are determined by simultaneously fitting to the $\delta(r^2)$ and $\Delta(r^2)$ data and they are found to be $\gamma_1=0.3$ fm^2, $\gamma_2=0.025$ fm^2, and $\gamma_3=0$ fm^2. The results obtained with this parameter set for the isomer shift $\delta(r^2)$ and isotope shift $\Delta(r^2)$ are shown in Figs. 1(g) and 1(h), respectively. The present calculations reproduce the observed trends, i.e., the sudden drop in isomer shift and a rise followed by a drop of the isotope shifts in the phase-transition domain.

F. Two-nucleon transfer intensities

The first study of TNT, in *g*IBM framework, was by Akiyama *et al.* [14]. In this paper, TNT intensities are calculated using the stripping and pickup operators [29] (for $l=0$ transfer) $P^{(0)}_{\pm\rho}$, where

$$P^{(0)}_{+\rho}=\alpha_{+\rho}\sqrt{\hat{N}_\rho/\hat{N}}\,s^\dagger\left[\Omega_\rho-\hat{N}_\rho-\frac{\hat{N}_\rho}{\hat{N}}(\hat{n}_d+\hat{n}_g)\right]^{1/2} , \tag{12}$$

$$P^{(0)}_{-\rho}=\alpha_{-\rho}\left[\Omega_\rho-\hat{N}_\rho-\frac{\hat{N}_\rho}{\hat{N}}(\hat{n}_d+\hat{n}_g)\right]^{1/2} s\sqrt{\hat{N}_\rho/\hat{N}} . \tag{13}$$

Here $\rho=\pi$ (ν) for protons (neutrons) and $\Omega_{\pi(\nu)}$ is the proton (neutron) pair degeneracy. In the present calculations Ω_ν is taken to be $(126-82)/2=22$ and $\Omega_\pi=(82-50)/2=16$. The factor $\hat{N}_{\nu(\pi)}/\hat{N}$ counts the fraction of neutrons (protons) and $\alpha_{\pm\rho}$ are the free parameters. The cutoff factors in the transfer operators $P^{(0)}_{\pm\rho}$ in (12) and (13) are derived using the Otsuka-Arima-Iachello (OAI) mapping [30] procedure. Following Scholten *et al.* [18], the calculated two-nucleon transfer intensities are assumed to be proportional to the transfer cross sections,

$$\sigma_{\pm\nu}=(\zeta_{\pm\nu})|\langle \|(\alpha_{\pm\nu})^{-1}P^{(0)}_{\pm\nu}\|\rangle|^2 \ . \tag{14}$$

The parameters $\zeta_{\pm\nu}$ are determined to be $\zeta_{+\nu}=0.01$ mb/sr and $\zeta_{-\nu}=0.02$ mb/sr, by fitting to the data. These parameters are consistent with those of Scholten *et al.* [18]. It is to be noted that in general the knowledge of the kinematic factors is required to deduce the values of $\alpha_{\pm\nu}$ in Eqs. (12) and (13) from $\zeta_{\pm\nu}$ parameters in Eq. (14). The comparison with experimental (t,p) and (p,t) cross sections for the transfer to ground state 0_1^+ and the excited 0_2^+ states are shown in Figs. 1(i)–1(l). In both theory and experiment the transition is manifested as a drop in the ground-state transition and the corresponding increase in the $0_1^+\rightarrow 0_2^+$ transition strength (see also Fig. 4).

G. Summary and comments

Some comments on the results given in Secs. II A–II F are in order.

(i) The agreements shown in Figs. 1(a)–1(l) demonstrate that matrix diagonalization in a truncated *sdg* spherical basis is well suited for describing the structure of complex nuclei.

(ii) Scholten *et al.* [18] calculated in *sd* space, with neutron-number-dependent d-boson energies, all the observables given in Figs. 1(a)–1(l); the *sdg* results are obtained with comparatively less free parameters and the agreements are, in general, better.

(iii) The results show that the agreements obtained by OS in their *sdg* studies (with variational methods) for energies and $E2$'s extend to all other observables. The spherical basis calculations of all the observables is equally easy, which may not be the case with variational methods.

(iv) In all the calculations two sets of (F,κ) are employed, while OS employed only one fixed set. This need not be considered a drawback of the spherical basis because of (i) above and the fact that neither calculation reproduces the β- and γ-band energies and other related properties; see below.

(v) The simple Hamiltonian given in (1) produces β- and γ-band energies ~ 1 MeV higher than the data and that is also the case with OS calculations [19]. This calls for a more elaborate Hamiltonian and, with this, reliable predictions for $E4$ distributions and other detailed properties can be made. The results of these calculations are discussed below.

III. EXTENDED CALCULATIONS

In order to obtain a consistently good description of the ground-state, β, and γ bands in Sm isotopes calculations in the spherical basis are carried out employing a Hamiltonian that interpolates various gIBM dynamical symmetries [SU(3), SU(5), SU(6) and O(15)] [7,10],

$$
\begin{aligned}
&H=\varepsilon_d\hat{n}_d+\varepsilon_g\hat{n}_g+\alpha_1[H(\mathrm{SU}(3))]+\alpha_2[H(\mathrm{SU}(5))]+\alpha_3[H(\mathrm{SU}(6))]+\alpha_4[H(\mathrm{O}(15))]+\alpha_5[H(\mathrm{O}(3))]\ ,\\
&H(\mathrm{SU}(3))=-\tfrac{28}{5}Q^2\cdot Q^2\ ,\quad H(\mathrm{SU}(5))=-4\{G^2\cdot G^2+G^4\cdot G^4\}\ ,\\
&G^2=\sqrt{\tfrac{1}{5}}\{(s^\dagger\tilde{d}+d^\dagger\tilde{s})^2-\tfrac{3}{14}\sqrt{5}(d^\dagger\tilde{d})^2+\tfrac{6}{7}(d^\dagger\tilde{g}+g^\dagger\tilde{d})^2+\tfrac{3}{14}\sqrt{110}(g^\dagger\tilde{g})^2\}\ ,\\
&G^4=\sqrt{\tfrac{1}{5}}\{(s^\dagger\tilde{g}+g^\dagger\tilde{s})^4+\tfrac{2}{7}\sqrt{5}(d^\dagger\tilde{d})^4+\tfrac{5}{7}\sqrt{\tfrac{11}{2}}(d^\dagger\tilde{g}+g^\dagger\tilde{d})^4+\tfrac{1}{14}\sqrt{143}(g^\dagger\tilde{g})^4\}\ ,\\
&H(\mathrm{SU}(6))=-4\{h^2\cdot h^2+h^4\cdot h^4\}\ ,\qquad (15)\\
&h^2=-\frac{1}{\sqrt{6}}(s^\dagger\tilde{d}+d^\dagger\tilde{s})^2+\frac{5}{7\sqrt{6}}(d^\dagger\tilde{d})^2-\frac{9}{14\sqrt{2}}(d^\dagger\tilde{g}+g^\dagger\tilde{d})^2-\tfrac{1}{14}\sqrt{33}(g^\dagger\tilde{g})^2\ ,\\
&h^4=-\frac{1}{\sqrt{6}}(s^\dagger\tilde{g}+g^\dagger\tilde{s})^4-\tfrac{3}{14}\sqrt{\tfrac{5}{2}}(d^\dagger\tilde{d})^4-\tfrac{1}{14}\sqrt{\tfrac{55}{3}}(d^\dagger\tilde{g}+g^\dagger\tilde{d})^4+\tfrac{1}{14}\sqrt{\tfrac{143}{2}}(g^\dagger\tilde{g})^4\ ,\\
&H(\mathrm{O}(15))=I^2\cdot I^2+I^4\cdot I^4\ ,\quad I^2=(s^\dagger\tilde{d}+d^\dagger\tilde{s})^2,\quad I^4=(s^\dagger\tilde{g}+g^\dagger\tilde{s})^4\ ,\\
&H(\mathrm{O}(3))=\mathbf{L}\cdot\mathbf{L}\ ,\quad \mathbf{L}=\sqrt{10}\{(d^\dagger\tilde{d})^1+\sqrt{6}(g^\dagger\tilde{g})^1\}\ .
\end{aligned}
$$

The quadrupole operator Q^2 appearing in (15) is already defined in (2). It is worth mentioning that Hamiltonians $H(G), G=\mathrm{SU}(3)$, SU(5), SU(6), O(15), and O(3), are expressible in terms of the Casimir operators of the group G and the various subgroups that appear in the group chain defined by G [10,11]. Moreover the operators (G^2,h^2,I^2) and (G^4,h^4,I^4) are the quadrupole and hexadecupole generators of (SU(5), SU(6), O(15)) groups, respectively. The geometric shapes that correspond to the various dynamical symmetry groups of gIBM are studied [11] via coherent state formalism and they show that the groups SU(3) and SU(5) are relevant for deformed nuclei and SU(6) and O(15) groups for γ-unstable nuclei. Based on this consideration, the strength α_3 of $H(\mathrm{SU}(6))$ is set to 0. Thus the Hamiltonian given in (15) has six free parameters and they are determined by least-square fit to the spectra. The spectra for ^{148}Sm, ^{150}Sm, ^{152}Sm, and ^{154}Sm, $E4$ strength distributions for ^{152,154}Sm, Burke's [33] ratio (defined below) $\mathcal{R}$ for TNT, and properties of 1_1^+ states in ^{152,154}Sm are given below.

The spectra for ^{148}Sm, ^{150}Sm, ^{152}Sm, and ^{154}Sm are shown in Fig. 2, the rms deviation (from experiment) is 108, 74, 49, and 20 keV, respectively. The parameters obtained from the fits are $\varepsilon_d=0.9$ MeV, $\varepsilon_g=1.95$ MeV, $\alpha_1=3.87$ keV, $\alpha_2=2$ keV, $\alpha_3=0$ keV, $\alpha_4=6.17$ keV, and $\alpha_5=8.55$ keV for ^{148}Sm; $\varepsilon_d=0.62$ MeV, $\varepsilon_g=1.45$ MeV, $\alpha_1=1.95$ keV, $\alpha_2=3.4$ keV, $\alpha_3=0$ keV, $\alpha_4=6.52$ keV, and $\alpha_5=2.41$ keV for ^{150}Sm; $\varepsilon_d=0.7$ MeV, $\varepsilon_g=1.2$ MeV, $\alpha_1=3.44$ keV, $\alpha_2=16.68$ keV, $\alpha_3=0$ keV, $\alpha_4=30.24$ keV, and $\alpha_5=11.95$ keV for ^{152}Sm; $\varepsilon_d=0.7$ MeV, $\varepsilon_g=1.2$ MeV, $\alpha_1=4.47$ keV, $\alpha_2=8.46$ keV, $\alpha_3=0$ keV, $\alpha_4=31.17$ keV, and $\alpha_5=9.75$ keV for ^{154}Sm. As the $H(G)$ in (15) are in multipole-multipole form they contribute to the d and g boson energies. Adding this contribution, the $(\varepsilon_d,\varepsilon_g)$ values given above change to (0.90,2.11), (0.58,1.46), (0.48,1.18), and (0.42,1.10) MeV for ^{148}Sm, ^{150}Sm, ^{152}Sm, and ^{154}Sm, respectively. These $(\varepsilon_d,\varepsilon_g)$ values show a gradual decrease as we go from ^{148}Sm to ^{154}Sm and this is a characteristic feature of spherical-deformed transition. The α's for the vibrational ^{148}Sm and transitional ^{150}Sm nuclei are somewhat different from each other and they both are different (the significant difference is in α_2, α_4 values) from those of the rotational ^{152}Sm and ^{154}Sm nuclei; the parameters for the latter two nuclei are close to each other as expected.

From the parameter sets given above, it appears that the strength of $H(\mathrm{O}(15))\gg H(\mathrm{SU}(5))\gg H(\mathrm{SU}(3))$ and it leads to a misleading conclusion that SU(3) is not important for Sm isotopes while O(15) is more relevant; for ^{148,150}Sm the differences in the strengths are not very large. The problem here is that the basic operators all do not have the same normalization. In order to have a proper comparison, a measure for the norm (size) of the operator has to be used. One such measure is given by French [34] and it is employed in this paper. Appendix A gives the definition and expressions for the norms $\|H\|_m$ in m-boson space. Equation (A9) gives the following results:

$$
\begin{aligned}
&\|H(\mathrm{SU}(3))\|_{N=10}\simeq 4.2\|H(\mathrm{SU}(5))\|_{N=10}\ ,\\
&\|H(\mathrm{SU}(3))\|_{N=10}\simeq 10\|H(\mathrm{O}(15))\|_{N=10}\ ,\\
&\|H(\mathrm{SU}(3))\|_{N=10}\simeq 8\|H(\mathrm{SU}(6))\|_{N=10}\ ;
\end{aligned}
$$

$N=10$ corresponds to ^{152}Sm. They clearly demonstrate that the parameters α's are meaningful and all the interactions $\alpha_1 H(\mathrm{SU}(3))$, $\alpha_2 H(\mathrm{SU}(5))$, and $\alpha_4 H(\mathrm{O}(15))$ are, globally, roughly of the same size. Similar results are obtained for $N=8$, 9, and 11 appropriate for ^{148}Sm, ^{150}Sm, and ^{154}Sm.

The Hamiltonian in (15), with the parameters given above, not only provides a good description of ground-

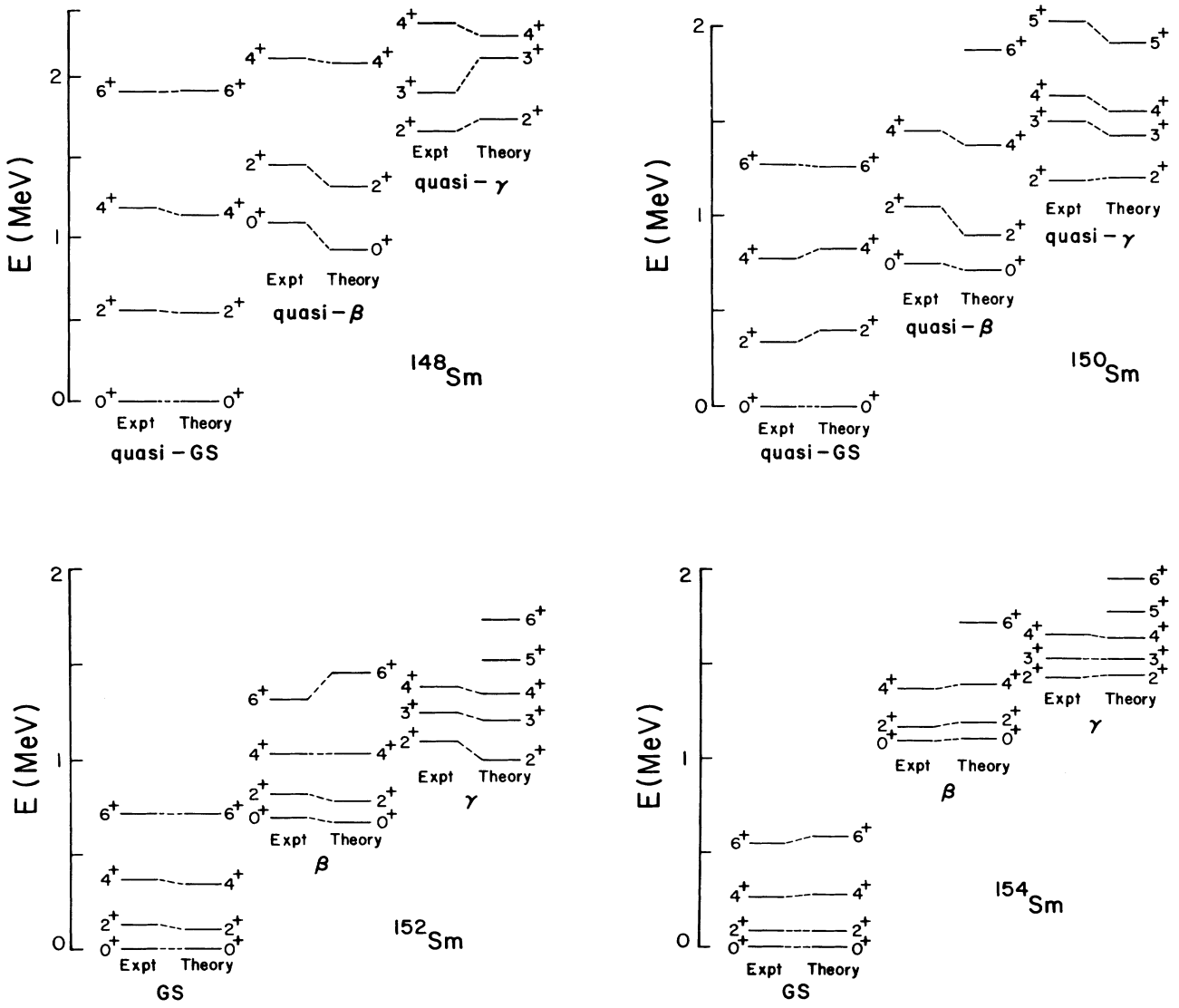

FIG. 2. Comparison between calculated (theory) and experimental (expt) low-lying energy levels [18,21] in g.s., β-, and γ-bands in ^{148}Sm, ^{150}Sm, ^{152}Sm , and ^{154}Sm; note that GS in the figures stands for g.s. As the nuclei ^{148,150}Sm are not deformed, the g.s., β, and γ bands in these nuclei are labeled quasi-g.s., quasi-β, and quasi-γ bands, respectively. See text (Sec. III) for the Hamiltonian and the corresponding parameters. The matrix dimensions are given in Table I.

state, β, and γ bands but also keeps intact all the results reported in Sec. II. It should be mentioned here that the $B(E2)$'s from β- and γ-band members to ground state 0^+, which are smaller (see Ref. [18]) by a factor of 100 compared to $B(E2;2_1^+ \rightarrow 0_1^+)$, are well described by the calculations.

More strikingly, using the $E4$ operator given in (7) with the effective charge $e_4 = 0.034\ e\ \mathrm{b}^2$ as determined by fitting $B(E4;0_1^+ \rightarrow 4_1^+)$ data, the predicted values for $B(E4;0_1^+ \rightarrow 4_\gamma^+)$ are 0.014 $e^2\mathrm{b}^4$ for ^{152}Sm and 0.014 $e^2\mathrm{b}^4$ for ^{154}Sm [note that ^{148,150}Sm are not dealt with as $B(E4)$ data for these nuclei are not available]. They are in excellent agreement with the recent[1] B(IS4) data (0.011 and 0.012 $e^2\mathrm{b}^4$) of Ichihara *et al.* [3]. With this agreement, $E4$ distributions in ^{152,154}Sm are predicted and the results are given in Fig. 3. The distributions given in the figure

[1] B(IS4) is isoscalar hexadecupole transition strength and in Ref. [3] their values are determined from the analysis of data from inelastic scattering experiments with 65 MeV polarized protons. As in Ref. [2] and elsewhere, in the present paper B(IS4)'s are taken to be the same as $B(E4)$'s and compared with *g*IBM predictions.

are quite similar to the ones (both data and theory) in ^{150}Nd and ^{156}Gd reported by Wu *et al.* [4]; experimental data for Sm isotopes are not yet available.

Recently Burke [33] argued that the ratio $\mathcal{R}$ of the sum of the TNT cross sections to excited 0^+ states to that of the ground state 0^+ provides a good test of nuclear models. Moreover, the cross-section ratio can be approximated by the corresponding ratio involving TNT strengths:

$$\mathcal{R}_{\pm\nu}=\frac{\sum_{\text{exc}\neq\text{g.s.}} |\langle 0^+_{\text{exc}}\|P_{\pm\nu}\|0^+_{\text{g.s.}}\rangle|^2}{|\langle 0^+_{\text{g.s.}}\|P_{\pm\nu}\|0^+_{\text{g.s.}}\rangle|^2} . \quad (16)$$

The (t,p) and (p,t) data for $\mathcal{R}$ in the entire rare-earth region is compiled [33,35]. The (t,p) data show prominent peaks at neutron numbers 90, 108, and (p,t) data at 88. Dynamical symmetries of *g*IBM explain [29,35] the average $\mathcal{R}$ value reasonably well all across the $\mathcal{N}=82-126$ region but they fail to predict the peaks. In Sm isotopes the peak at neutron number 90 is due to spherical-deformed phase transition; the value of $\mathcal{R}$ changes from vibrational [$SU_{sd}(5)$] $\mathcal{R}=0$ to rotational [$SU_{sdg}(3)$]

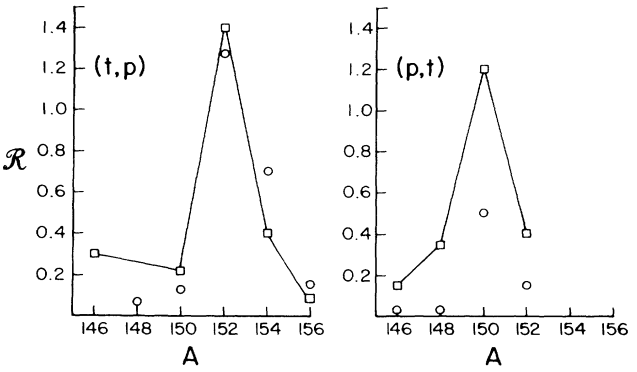

FIG. 4. Comparison of the ratio $\mathcal{R}$ of the sum of the cross sections to the excited 0^+ states to that of the ground state 0^+ for (t,p) and (p,t) reactions. The circles are calculated values and boxes are from experimental data [33,35]. The ratio $\mathcal{R}$ is given for the final nucleus A. All the *g*IBM results (except for ^{152}Sm⇆^{154}Sm) are obtained using the simple two-parameter interpolating Hamiltonian (1) of Sec. II. For ^{152}Sm⇆^{154}Sm the wave functions obtained by diagonalizing a more general *g*IBM Hamiltonian (see Sec. III) are used.

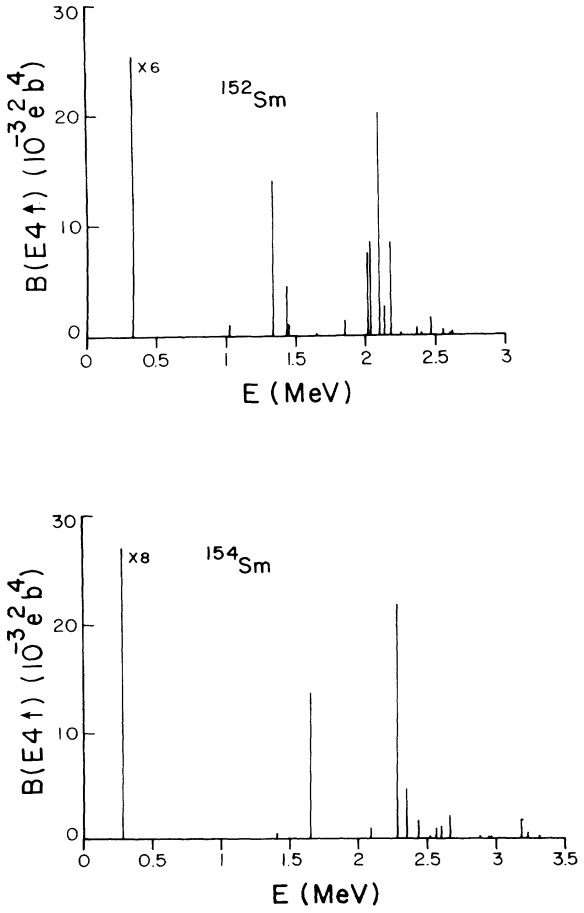

FIG. 3. $E4$ strength distributions in ^{152}Sm and ^{154}Sm. The $B(E4\uparrow)=B(E4;0^+_1\rightarrow 4^+_i)$ values for the 4^+_1 level are to be multiplied by a factor of 6 for ^{152}Sm and factor of 8 for ^{154}Sm. The $E4$ transition operator and the corresponding effective charges are given in Sec. II D.

$\mathcal{R}=4/N\simeq 0.3$ value. The Hamiltonian in (1) predicts the peak very well [as it interpolates $SU_{sd}(5)$ and $SU_{sdg}(3)$], but the values for ^{152}Sm⇆^{154}Sm are much smaller than the experimental values. For these transitions, the value of $\mathcal{R}$ is recalculated using the wave functions given by the Hamiltonian (15) and the results are shown in Fig. 4. In using (16), the cutoff factors appearing in $P_{\pm\nu}$ [see (12), (13)] are ignored as we are dealing with a ratio. One sees that the detailed numerical calculations reproduce the observed variation in $\mathcal{R}$ very well; for (p,t) the predicted peak value is somewhat smaller.

In *g*IBM one can generate 1^+ levels, which is not possible with s and d bosons alone. With the Hamiltonian (15), the 1^+_1 levels appearing at 1.91 and 2.01 MeV in the rotational nuclei ^{152}Sm and ^{154}Sm, respectively, and the $B(M1;0^+_1\rightarrow 1^+_1)=B(M1\uparrow)$ value, with the $M1$ operator and the corresponding g factors given in Sec. II C, are predicted to be $0.10\mu_N^2$ and $0.15\mu_N^2$, respectively. In ^{154}Sm the scissors [36] 1^+ level is observed at 3.2 MeV with $B(M1\uparrow)\simeq(0.8\pm0.2)\mu_N^2$, and obviously it cannot be the *g*IBM 1^+_1 level. Therefore it would be interesting to look for 1^+_1 levels around 2 MeV in ^{152,154}Sm; see also Ref. [37].

IV. CONCLUSIONS

First systematic calculations for a series of isotopes in *sdg*IBM framework are presented in this article with Sm isotopes, which exhibit spherical-deformed phase transition, as the example. It is clearly demonstrated that the spherical basis with a symmetry-defined Hamiltonian with few free parameters (not much more than what one has in *sd*IBM) describes the spectroscopic data rather well, the former is well confirmed in Sec. II, and the latter (together with the former) by the results in Sec. III. Similar successful calculations for isotopes in the Os-Pt region

(where good $E4$ data are available [1]) are also carried out and the results will appear elsewhere [38]. These studies establish that *g*IBM is a simple yet powerful tool in analyzing and predicting $E4$ properties in atomic nuclei. Finally we mention that the important problem of understanding and derivation of parameters in the Hamiltonian and various transition operators is postponed to a future publication.

ACKNOWLEDGMENTS

Thanks are due to A. Sen for providing facilities at the Institute for Plasma Research (Gandhinagar, India) where all the computational work is carried out. We thank R. K. Varma (Physical Research Laboratory) for financial assistance towards obtaining computation time.

APPENDIX A

Let us start with a one- + two-body Hamiltonian:

$$H = h + V \ , \tag{A1}$$

where $h = \sum_l \varepsilon_l \hat{n}_l$ is the one-body Hamiltonian and the interaction V is defined in terms of the matrix elements $V^L_{l_1 l_2 l_3 l_4} = \langle (l_1 l_2) L | V | (l_3 l_4) L \rangle$. In *sdg* boson space l's stand for s, d, and g. The Hamiltonain H can be decomposed into tensors with respect to the U($\mathcal{N}$) group [39], where $\mathcal{N} = \sum_l \mathcal{N}_l$ and $\mathcal{N}_l = 1$, 5, and 9 for s, d, and g, respectively. Thus

$$H = H^{\omega=0} + H^{\omega=1} + H^{\omega=2} \ , \quad H^{\omega=0} = h^{\omega=0} + V^{\omega=0} \ , \tag{A2}$$

$$H^{\omega=1} = h^{\omega=1} + V^{\omega=1} \ , \quad H^{\omega=2} = V^{\omega=2} \ ,$$

where ω is the tensorial rank with respect to U($\mathcal{N}$) group which is U(15) in *sdg* case. Using the results of Ref. [39] we have

$$h^{\omega=0} = \bar{\varepsilon}\hat{n} \ , \quad \bar{\varepsilon} = \frac{1}{\mathcal{N}} \sum_l \mathcal{N}_l \varepsilon_l \ , \tag{A3}$$

$$h^{\omega=1} = \sum_l \tilde{\varepsilon}_l \hat{n}_l \ , \quad \tilde{\varepsilon}_l = \varepsilon_l - \bar{\varepsilon} \ , \tag{A4}$$

$$V^{\omega=0} = \bar{V} \begin{bmatrix} \hat{n} \\ 2 \end{bmatrix} \ ,$$

$$\bar{V} = \left\{ \sum_{l_1 \geq l_2} V^L_{l_1 l_2 l_1 l_2} (2L+1) \right\} \left\{ \frac{\mathcal{N}(\mathcal{N}+1)}{2} \right\}^{-1} \ , \tag{A5}$$

$$V^{\omega=1} = \frac{\hat{n}-1}{\mathcal{N}+2} \sum_l \tilde{\lambda}_l \hat{n}_l \ ,$$

$$\tilde{\lambda}_l = \frac{1}{\mathcal{N}_l} \sum_{l'} V^L_{ll'll'} (2L+1)(1+\delta_{ll'}) - (\mathcal{N}+1)\bar{V} \ . \tag{A6}$$

The $\tilde{\lambda}_l$'s are known as traceless induced single-particle energies. Finally the $V^{\omega=2}$ is defined by $\tilde{V}^L_{l_1 l_2 l_3 l_4}$ for $l_1 \geq l_2$, $l_3 \geq l_4$:

$$\tilde{V}^L_{l_1 l_2 l_3 l_4} = V^L_{l_1 l_2 l_3 l_4} - \left\{ \bar{V} + \frac{1}{\mathcal{N}+2} (\lambda_{l_1} + \lambda_{l_2}) \right\} \delta_{l_1 l_3} \delta_{l_2 l_4} \ . \tag{A7}$$

The norm $\|O\|_m$ of an operator O in m-particle space is defined as

$$\|O\|_m = [\langle (\tilde{O})^2 \rangle^m]^{1/2} = \{ \langle [O - \langle O \rangle^m]^2 \rangle^m \}^{1/2} \ , \tag{A8}$$

where the symbol $\langle \ \rangle$ stands for m-particle space average. The norms of various parts of the operator H can be written down in the m-boson spaces using the following trace propagation [34,39] equations:

$$\|H\|^2_m = \|H^{\omega=1}\|^2_m + \|H^{\omega=2}\|^2_m \ ,$$

$$\|H^{\omega=1}\|^2_m = \frac{m(\mathcal{N}+m)}{\mathcal{N}(\mathcal{N}+1)} \sum [\xi_l(m)]^2 \mathcal{N}_l \ ,$$

$$\|H^{\omega=2}\|^2_m = \|V^{\omega=2}\|^2_m = \frac{m(m-1)(\mathcal{N}+m)(\mathcal{N}+m+1)}{\mathcal{N}(\mathcal{N}+1)(\mathcal{N}+2)(\mathcal{N}+3)} \langle\langle (V^{\omega=2})^2 \rangle\rangle^2 \ ,$$

$$\langle\langle (V^{\omega=2})^2 \rangle\rangle^2 = \sum_{\substack{l_1 \geq l_2 \\ l_3 \geq l_4; L}} (\tilde{V}^L_{l_1 l_2 l_3 l_4})^2 (2L+1) \ . \tag{A9}$$

In (A9) $\xi_l(m) = \tilde{\varepsilon}_l + [(m-1)/(\mathcal{N}+2)]\tilde{\lambda}_l$ and the symbol $\langle\langle \ \rangle\rangle$ stands for the m-particle trace.

[1] A. Sethi, F. Todd Baker, G. T. Emery, W. P. Jones, and M. A. Grimm, Nucl. Phys. **A518**, 536 (1990); F. Todd Baker, A. Sethi, V. Penumetcha, G. T. Emergy, W. P. Jones, M. A. Grimm and M. L. Whitten, Phys. Rev. C **32**, 2212 (1985).

[2] I. M. Govil, H. W. Fulbright, and D. Cline, Phys. Rev. C **36**, 1442 (1987); I. M. Govil, H. W. Fulbright, D. Cline, E. Wesolowski, B. Kotlinski, A. Backlin, and K. Gridnev, *ibid.* **33**, 793 (1986).

[3] T. Ichihara, H. Sakaguchi, M. Nakamura, M. Yosoi, M.

Yeiri, Y. Tekeuchi, H. Yogawa, T. Tsutsumi, and S. Kobayashi, Phys. Rev. C **36**, 1754 (1987).
[4] H. C. Wu, A. E. L. Dieperink, O. Scholten, M. N. Harakeh, R. De Leo, M. Pignanelli, and I. Morrison, Phys. Rev. C **38**, 1638 (1988).
[5] R. De Leo, N. Blassi, S. Micheletti, M. Pignanelli, W. T. A. Borghols, J. M. Schippers, S. Y. Vader Werf, G. Maino, and M. N. Harakeh, Nucl. Phys. **A504**, 109 (1989).
[6] Y. Fujita, M. Fujiwara, S. Morinobu, I. Katayama, T. Yamazaki, T. Itahashi, H. Ikegami, and S. I. Hayakawa, Phys. Rev. C **40**, 1595 (1989).
[7] Y. D. Devi and V. K.B. Kota, Physical Research Laboratory Report PRL-TN-90-68, 1990 (Ahmedabad, India); Y. D. Devi, V. K. B. Kota, and J. A. Sheikh, Phys. Rev. C **39**, 2057 (1989).
[8] Y. D. Devi and V. K. B. Kota, J. Phys. G **17**, 465 (1991); P. Van Isacker, K. Heyde, M. Waroquier, and G. Wenes, Nucl. Phys. **A380**, 383 (1982).
[9] J. Dukelsky, J. F. Niello, H. M. Sofia, and R. P. J. Perrazo, Phys. Rev. C **28**, 2183 (1983).
[10] V. K. B. Kota, H. De Meyer, J. Vander Jeugt, and G. Vanden Berghe, J. Math. Phys. **28**, 1644 (1987).
[11] Y. D. Devi and V. K. B. Kota, Z. Phys. A **337**, 15 (1990).
[12] H.C. Wu, A. E. L. Dieperink, and S. Pittel, Phys. Rev. C **34**, 703 (1986); N. Yoshinaga, Nucl. Phys. **A456**, 21 (1986); Y. Akiyama, *ibid.* **A433**, 369 (1985); R. D. Ratna Raju, Phys. Rev. C **23**, 518 (1981).
[13] N. Yoshinaga, Y. Akiyama, and A. Arima, Phys. Rev. Lett. **56**, 1116 (1986); Phys. Rev. C **38**, 419 (1988).
[14] Y. Akiyama, K. Heyde, A. Arima, and N. Yoshinaga, Phys. Lett. B **173**, 1 (1986).
[15] S. Kuyucack and I. Morrison, Ann. Phys. (N.Y.) **181**, 79 (1988); Phys. Rev. Lett. **58**, 315 (1987).
[16] T. Otsuka and M. Sugita, Phys. Lett. B **215**, 205 (1988).
[17] N. Yoshinaga, Nucl. Phys. **A503**, 65 (1989); H. T. Chen, L. L. Kiang, C. C. Yang, L. M. Chen, T. L. Chen, and C. W. Jiang, J. Phys. G **12**, L217 (1986).
[18] O. Scholten, F. Iachello, and A. Arima, Ann. Phys. (N.Y.) **115**, 325 (1978); O. Scholten, Ph.D. thesis, University of Groningen (1980).
[19] T. Otsuka (private communication); N. Yoshinaga, Nucl. Phys. **A522**, 99c (1991).
[20] W. Pannert, P. Ring, and Y. K. Gambhir, Nucl. Phys. **A443**, 189 (1985).
[21] *Table of Isotopes,* 7th ed., edited by C. M. Lederer and V. S. Shirley (Wiley, New York, 1978); Nuclear Data Sheets **59**, 393 (1990).
[22] A. H. Wapstra and K. Bos, At. Data Nucl Data Tables **19**, 175 (1977).
[23] S. Raman, C. H. Malarkey, W. T. Milner, C. W. Nestor, Jr., and P. H. Stelson, At. Data Nucl. Data Tables **36**, 1 (1987).
[24] R. J. Powers, P. Barreau, B. Bihoreau, J. Miller, J. Morgenstern, J. Picard, and L. Roursel, Nucl. Phys. **A316**, 295 (1979).
[25] H. W. Kugel, R. R. Borchers, and R. Kalish, Nucl. Phys. **A186**, 513 (1972).
[26] T. Cooper, W. Bertozzi, J. Heisenberg, S. Kowalski, W. Turchinetz, C. Williamson, L. Cardman, S. Fivozinsky, J. Lightbody, Jr., and S. Penner, Phys. Rev. C **13**, 1083 (1976).
[27] G. M. Kalvius and G. K. Shenoy, Nucl. Data Tables **14**, 639 (1974).
[28] P. L. Lee and F. Boehm, Phys. Lett. **35B**, 33 (1971).
[29] V. K. B. Kota and Y. D. Devi, J. Phys. G **17**, L185 (1991).
[30] T. Otsuka, A. Arima, and F. Iachello, Nucl. Phys. **A309**, 1 (1978).
[31] J. H. Bjerregaard, O. Hansen, O. Nathan, and S. Hinds, Nucl. Phys. **86**, 145 (1966).
[32] P. Debenham and N. M. Hintz, Nucl. Phys. **A195**, 385 (1972).
[33] D. G. Burke (private communication).
[34] F. S. Chang, J. B. French, and T. H. Thio, Ann. Phys. (N.Y.) **66**, 137 (1971).
[35] P. E. Garrett, D. G. Burke, Y. D. Devi, and V. K. B. Kota, Book of Abstracts, Symposium in Honour of A. Arima, 1990, Santa Fe, New Mexico, p. 57.
[36] U. Hartmann, D. Bohle, T. Guhr, K. D. Hummel, G. Kilgus, U. Milkau, and A. Richter, Nucl. Phys. **A465**, 25 (1987).
[37] I. Morrison, P. von Brentano, and A. Gelberg, J. Phys. G **15**, 801 (1989).
[38] Y. D. Devi and V. K. B. Kota, Physical Research Laboratory Report PRL-TH-91-26, 1991.
[39] V. K. B. Kota and V. Potbhare, Phys. Rev. C **21**, 2637 (1980); V. K. B. Kota, Ann. Phys. (N.Y.) **134**, 221 (1981).